Princeton Plasma Physics Laboratory

PPPL- 4785

PPPL- 4785

Geometrical Constraints on Plasma Couplers for Raman Compression

Z. Toroker, V.M. Malkin, G.M. Fraiman, A.A. Balakin, and N.J. Fisch

July, 2012

PPPL PRINCETON PLASMA PHYSICS LABORATORY

Prepared for the U.S. Department of Energy under Contract DE-AC02-09CH11466.

Princeton Plasma Physics Laboratory
Report Disclaimers

Full Legal Disclaimer

Trademark Disclaimer

PPPL Report Availability

Princeton Plasma Physics Laboratory:

http://www.pppl.gov/techreports.cfm

Office of Scientific and Technical Information (OSTI):

http://www.osti.gov/bridge

Related Links:

U.S. Department of Energy

Office of Scientific and Technical Information

Fusion Links

Geometrical Constraints on Plasma Couplers for Raman Compression

Z. Toroker,[1] V. M. Malkin,[2] G. M. Fraiman, A. A. Balakin,[3] and N. J. Fisch[1]
[1)] *Princeton Plasma Physics Laboratory, Princeton, NJ USA 08543*
[2)] *Department of Astrophysical Sciences, Princeton University, Princeton, NJ USA 08544*
[3)] *Institute of Applied Physics RAS, Nizhnii Novgorod, Russia 603950*

(Dated: 15 May 2012)

Backward Raman compression in plasma is based on a 3-wave resonant interaction, which includes two-counter propagating laser pulses (pump and seed pulses) and an electron plasma wave (Langmuir wave). A high-density, roughly homogeneous, plasma mediates the energy transfer between the lasers by ensuring resonance with the plasma wave. However, in practice, a laser pulse entering or leaving plasma source encounters plasma at the edges of the homogeneous section that is far too tenuous to maintain resonance. When these tenuous plasma regions are extensive, such as for the wider plasma necessary for compression at higher powers, significant inverse bremsstrahlung and seed dispersion may occur. These deleterious effects may, however, be mitigated by chirping the seed and pump pulses.

I. INTRODUCTION

Resonant backward Raman amplification[1] (BRA) in plasma may enable the next generation high intensity laser pulses. In this approach, the dielectric grating limitation of the chirped pulse amplification[2] (CPA) is overcome through the use of plasma medium.

The BRA scheme consists of two counter-propagating laser pulses, a long pump pulse and a short seed pulse, that propagate in a plasma medium. When the pulses begin to overlap, the long pump pulse transfers part of its energy to the short seed pulse via the mediation of the Langmuir wave. The most effective energy transfer occurs when the Raman resonance condition is satisfied. This mechanism continues to attract considerable attention, including theoretical, experimental, and computational, as well as extrapolation to regimes not originally contemplated[3–38].

However, in practical realizations of the plasma, there will be a homogeneous cross section flanked by inhomogeneous, tenuous plasma, end sections. For given pump and seed frequencies, the Raman resonance condition is then generally satisfied only in the homogeneous plasma section. The inhomogeneous sections do not help the compression effect, but could impede it.

While the assumption of homogeneity is appropriate for describing the first generation of Raman compression experiments[1,3–38], this assumption will not hold for the next generation of intensities. This is because the first generation of experiments is in the limit of what we can call *low aspect ratio plasma coupling*, where the plasma cross sectional dimension is small compared to the length of the homogeneous region. When this transverse dimension of the plasma is shorter than the longitudinal dimension, the tenuous-plasma end regions will likely be on the order of the transverse dimension, so the plasma coupler length will most probably be shorter than the length of the homogeneous section. Hence, in such structures it is generally justified to assume theoretically that the interaction is dominated by the physics of the central homogeneous region.

However, to achieve the next generation of intensities, significant transverse focusing will be required in addition to the longitudinal compression, so a large laser spot size will be required to process more power for the Raman compression. Yet, the length of the plasma homogeneous section remains fixed by other considerations[1], resulting in what might be called a *high aspect ratio* plasma coupling region. In the high-aspect ratio limit, the plasma is shaped like a pancake. But since the plasma transverse dimension is longer than its width, the falloff in density in the longitudinal direction (or laser propagation direction) is likely to occur over many plasma widths, giving rise to inhomogeneous sections of tenuous plasma longer than the homogeneous section. Hence, in the inhomogeneous regions where the plasma density does not satisfy the resonance condition, there is a concern that deleterious effects such as inverse bremsstrahlung and seed dispersion will reduce significantly the Raman compression.

To determine quantitatively how the tenuous inhomogeneous plasma regions can affect the Raman compression, we consider here a plasma slab that comprises a homogeneous middle section and two symmetrically placed inhomogeneous end sections, such that the electron density in each end section decreases to zero. We call the total length from each edge of the homogeneous section to the point where the plasma density decreases by half the *plasma coupler length*. The typical plasma coupler length is expected to be of the order of the transverse plasma dimension.

Here we show that, for plasma coupler length longer than the length of the homogeneous section, as we expect to find in the next generation of Raman compression experiments, the Raman compression tends to be significantly reduced due to the seed dispersion and the inverse bremsstrahlung. However, as we also show, chirping both the seed and the pump pulses can partially overcome the deleterious effects of both the dispersion and the inverse bremsstrahlung.

This paper is organized as follows: Section II describes the coupled 3-wave equations associated to the BRA and the electron heat equation, derived from a one dimensional fluid model. In Section III we show numerically

that the Raman amplification and efficiency is affected by both the plasma coupler length and the initial pump intensity. In Section IV we show that pump and seed chirping can partially overcome the deleterious seed dispersion and the inverse bremsstrahlung effects. Conclusions are given in Section V.

II. MODEL DESCRIPTION

The one dimensional normalized backward Raman compression model can be described by the coupled 3-wave equations:

$$\begin{aligned} a_t + a_z c_a/c &= q_n^{1/4} b f + i\sigma_a a - \nu_a a, \\ b_t - b_z c_b/c &= -q_n^{1/4} a f^* + i\sigma_b b - i\kappa b_{tt} + iR\left|b\right|^2 b - \nu_b b, \\ f_t &= -q_n^{1/4} a b^* + i\sigma_f f - \nu_f f, \end{aligned} \tag{1}$$

and the electron heat equation

$$\frac{\partial q_T}{\partial t} = \frac{2}{3}\left[\nu_{ei}\left(T_{ab}+T_f\right)/T_m + 2\nu_{Lnd}T_f/T_m\right], \tag{2}$$

where a and b are the normalized amplitudes of the circularly polarized vector potentials of the pump and the seed pulses such that the amplitudes of the vector potentials are measured in units of $a_0 m_e c^2/e$ and $\sqrt{\omega_a/\omega_b}a_0 m_e c^2/e$, respectively. Also, f is the normalized amplitude of the plasma wave electric field such that amplitude of the electric field is measured in units of $\sqrt{2\omega_a\omega_e}a_0 m_e c/e$. Here, the frequency of the pump laser and the seed laser are ω_a and ω_b, respectively. The electron plasma frequency is $\omega_e = \sqrt{4\pi n_h e^2/m_e}$, where m_e is the electron mass, e is the electron charge, n_h is the electron density in the homogeneous section and c is the speed of light in vacuum. The initial normalized pump amplitude is $a_0 = \lambda_a\sqrt{I_{a0}/\pi c}/m_e c^2/e \approx 6\cdot 10^{-6}\lambda_a\sqrt{I_{a0}}$, where λ_a is the pump wavelength measured in cm and I_{a0} is the initial pump intensity measured in W/cm^2.

The group velocity of the pump is $c_a = c\sqrt{1-\omega_e^2/\omega_a^2}$ and the group velocity of the seed is $c_b = c\sqrt{1-\omega_e^2/\omega_b^2}$. The time t is measured in units of $1/V_3 a_0$ and the distance z in units of $c/V_3 a_0$, where $V_3 = (k_f c/2)\sqrt{\omega_e/2\omega_b}$ is the 3-wave coupling constant[39]. The resonant Langmuir wave number, k_f, in the homogeneous section is $k_f = k_a + k_b$, where $k_a c = \sqrt{\omega_a^2-\omega_e^2}$ and $k_b c = \sqrt{\omega_b^2-\omega_e^2}$. The frequency resonance condition in the homogeneous section is $\omega_a = \omega_b + \omega_f$, where $\omega_f = \omega_e\sqrt{1+3q_T}$ is the resonant Langmuir frequency and $q_T = k_f^2 T_e/\omega_f^2 m_e = T_e/T_m$ is the electron temperature measured in T_m. We assume that the plasma is cold enough such that $\omega_f \approx \omega_e$.

The plasma inhomogeneity induces frequency shifts of $\sigma_a = \omega_e^2(q_n-1)/2V_3\omega_a$, $\sigma_b = \omega_e^2(q_n-1)/2V_3\omega_b$, and $\sigma_f = \omega_e^2(q_n-1)/2V_3\omega_f$ to the pump, seed, and Langmuir wave pulses, where $q_n = n_e(z)/n_h$ is the normalized electron density. The nonlinear frequency shift coefficient is $R = a_0\omega_e^2\omega_a q_n/V_3 4\omega_b^2$ due to the electron relativistic motion. For homogeneous plasma ($q_n = 1$) the coefficient R reduces to the same expression described in Refs. 19, 24, 40–42. The seed group velocity dispersion coefficient is $\kappa = \omega_e^2 q_n/[a_0 V_3 2\omega_b(\omega_b^2-\omega_e^2 q_n)]$. For homogeneous plasma ($q_n = 1$) the coefficient κ reducees to the same expression described in Refs. 19 and 24.

The inverse bremsstrahlung rates of the pump and seed pulses due to the electron-ion collision are $\nu_a = \nu_{ei}q_n\omega_e^2/2\omega_a^2$ and $\nu_b = \nu_{ei}q_n\omega_e^2/2\omega_b^2$. The electron-ion collision rate in inhomogeneous plasma is modeled[19,43,44] by

$$\nu_{ei} = \frac{1}{a_0 V_3}\frac{2}{3}\sqrt{\frac{2\pi}{m_e}}\frac{Z\Lambda n_h q_n e^4}{T_e^{1/2}(T_e+T_{ab}+T_f)}, \tag{3}$$

where $T_{ab} = m_e c^2 a_0^2\left(\left|a\right|^2+\left|b\right|^2\omega_a/\omega_b\right)$ and $T_f = m_e c^2 a_0^2\left|f\right|^2\omega_a/\omega_f$. Also, Λ is the Coulomb logarithm and Z is the ion state charge.

The Langmuir wave pulse damping rate, $\nu_f = \nu_{ei}/2 + \nu_{lnd}$, consists of both the electron-ion collision and the Landau damping rates. The linear Landau damping rate is modeled by

$$\nu_{lnd} = \frac{1}{a_0 V_3}\frac{\sqrt{\pi}\omega_e}{(2q_T)^{3/2}}q_n^4\exp\left[-\frac{q_n}{2q_T}-\frac{3}{2}\right]. \tag{4}$$

Note that for homogeneous plasma, $q_n = 1$, the model described here reduces to the same model as in Ref. 19. In the regime of homogeneous ($q_n = 1$) and collisionless plasma ($\nu_{ei} = 0$) with the assumptions that the Landau damping (ν_{lnd}), dispersion (κ) and cubic nonlinearity (R) terms can be neglected, the solution of Eq. (1) is well known[45–51].

III. NUMERICAL SIMULATIONS

To study the key features of the BRA in inhomogeneous plasma, we solve Eqs. (1) and (2) numerically. The electron density in the homogeneous section is $n_h = 10^{21}$ cm^{-3}, which corresponds to plasma wavelength $\lambda_e = 1.06$ μm. We consider an electron density profile, $q_n(z) = n(z)/n_h$, given by

$$q_n(z) = \begin{cases} e^{-\frac{(z-z_p)^2}{2(0.2z_p)^2}} & 0 \le z < z_p \\ 1 & z_p \le z \le (z_p+z_h) \\ e^{-\frac{(z-z_p-z_h)^2}{2(0.2z_p)^2}} & (z_p+z_h) < z \le z_{end}, \end{cases} \tag{5}$$

where Δ_n is the plasma coupler length, $z_h = 20.56\lambda_e = 21.8$ μm is the length of the homogeneous section, $z_p = \Delta_n/0.47$, and the total length of the plasma is $z_{end} = 2z_p + z_h$. The pump wavelength in vacuum is $\lambda_a = 0.351$ μm, corresponding to $\omega_e/\omega_a = 0.33$. Unless mentioned otherwise, the initial pump pulse intensity is $I_{a0} = I_{br} = 84.55$ PW/cm^2 ($a_0 = a_{br} = 0.0612$), where $a_{br} = (\omega_e/\omega_a)^{3/2}\omega_a/(2k_f c)$ is the pump amplitude and I_{br} is the pump intensity at the wavebreaking threshold[1,39]. The width of the rectangular pump pulse is $\Delta_a = z_h(1/c_a+1/c_b) \approx 0.16$ psec, which fit to BRA in the

homogeneous section. The initial seed pulse has a Gaussian profile with maximum intensity of 1.5 PW/cm^2 and full width at half maximum (FWHM) of $4\pi/\omega_e = 7.04$ fsec. Here, $\Lambda = 3.14$, $Z = 6$, and $T_e(t = 0, z) = 50$ eV ($q_T(t = 0, z) = 2.02 \cdot 10^{-3}$).

Figure 1 shows the evolution of the pump, seed, and Langmuir pulses, and the electron temperature, for $\Delta_n/z_h = 1$ (Figs. 1a and 1b) and $\Delta_n/z_h = 3$ (Fig. 1c). Only in Fig. 1b the initial pump intensity is 28.18 PW/cm^2, which is a third of the wavebreaking threshold. In all three cases, the BRA starts at the right edge of the homogeneous section and ends at the left edge of the homogeneous section. The seed amplitude at the plasma exit is smaller than at the edge of the homogeneous section, while at both the plasma exit and the edge of the homogeneous section the corresponding seed fluences remain almost the same. Thus, the amplification reduction is mainly due to the non-dissipative seed dispersion effect.

For longer plasma coupler length with the same initial pump, the seed amplification and dispersion at the edge of the homogeneous section will be almost the same. However, the seed passes through a longer plasma coupler with initial strong dispersion which, in turn, results in a longer distance over which the seed amplitude is reduced. It can be seen from Fig. 1b that, for $I_{a0} = I_{br}$ and $\Delta_n/z_h = 3$, the seed amplitude is reduced at the edge of the homogeneous section from about 4 to 2 at the plasma exit. In Fig. 1b the seed amplitude at the plasma exit is as small as the secondary spike, resulting in a non-focused pulse.

On the other hand, for smaller initial pump intensity, hence smaller Raman growth rate and for the same plasma coupler length, the total seed amplification at the edge of the homogeneous section will be smaller. The smaller seed amplification corresponds to a wider seed width which results in a smaller seed dispersion, so that the seed amplitude is hardly reduced in the plasma coupler exit. In our example, for $I_{a0} = I_{br}$ and $\Delta_n/z_h = 1$ (Fig. 1a) the seed amplitude is reduced at the edge of the homogeneous section from about 4 to 3 at the plasma exit, while for $I_{a0} = I_{br}/3$ and $\Delta_n/z_h = 1$ (Fig. 1c) the seed amplitude is reduced from about 2.7 to 2.5.

Figure 2 shows the local gain (Fig. 2a) and efficiency (Fig. 2b) for the cases shown in Fig. 1a (Fig. 2 solid curve) and Fig. 1c (Fig. 2 dashed-dot curve). The local gain of the seed is defined by

$$G(t) = \frac{I_b}{I_{a0}} = \frac{\omega_b}{\omega_a} \max_z |b(z,t)|^2 , \tag{6}$$

where I_b is the maximum seed intensity and the local efficiency of the seed is defined by

$$\eta(t) = \frac{W_b}{W_{a0}} = \frac{\omega_b}{\omega_a} \frac{\int_{-\infty}^{\infty} |b(z,t)|^2 \, dz}{\Delta_a}, \tag{7}$$

where W_b is the seed fluence and W_{a0} is the input pump fluence. In each time step we express the local gain and efficiency in terms of the maximum seed amplitude position i.e., $t = t(z_M)$, where z_M is the maximum seed amplitude position.

As Fig. 2a shows, the Raman amplification of the seed starts at the right side ($z \approx 60\lambda_e$) of the homogeneous section and ends at the left side ($z \approx 40\lambda_e$). At the left edge of the homogeneous section the seed amplitude is the largest but with the shortest duration. Hence, at this point the seed dispersion is the strongest. When the seed begins to pass through the plasma coupler exit (on the left side), where it is no longer resonant, it is affected only by dispersion and by inverse bremsstrahlung. Since in both cases the local efficiency in the plasma coupler exit region remains approximately the same (Fig. 2b), the most dominant effect for the seed amplitude reduction is due to the dispersion. As the seed propagates thorough the plasma coupler exit its amplitude is decreased, and, from conservation of energy, its pulse width grows. At the same time the plasma density is decreased. Hence, the dispersion effect becomes smaller as the seed transverses through the exit region. Note also that, Fig. 2 shows that for smaller initial pump intensity (dashed curve) the seed amplitude reduction should be smaller. As explained above, this is because at low amplitude the Raman compression is smaller, so for the same length of homogeneous section the seed width at the left edge of the homogeneous section will be wider. Hence, at this point the seed dispersion is smaller, which results in a smaller reduction in the seed amplitude as it propagates through the plasma coupler exit.

Fig. 3 shows, in our example, the correlation of the output seed gain (a), efficiency (b), and leading spike efficiency (c) to the plasma coupler length and the three initial pump intensity : $I_{a0} = I_{br}$ (solid curve), $I_{a0} = I_{br}/2$ (dash-dot curve), and $I_{a0} = I_{br}/3$ (dashed curve). The output intensity (d), fluence (e), and leading spike fluence (f) are also shown. Here, the leading spike fluence is defined by $W_s = I_{out}\Delta_{out}$, where Δ_{out} is the seed width at the plasma exit. The leading spike efficiency, $\mu = W_s/W_{a0}$, is define as the leading spike fluence to the input pump fluence ratio. Note that for $I_{a0} = I_{br}$ the leading spike fluence and efficiency are not shown because the output seed is non-focused, as shown for example in Fig. 1b.

For the three initial pump intensity shown in Fig. 3 the output gain, efficiency, and leading spike efficiency are decreased as the plasma coupler length is increased. As shown in Fig. 3a, while for $I_{a0} = I_{br}$ the gain reduction is the largest, it is the smallest for $I_{a0} = I_{br}/3$ due to the dispersion effect. The largest gain reduction occurs at $\Delta_n/z_h = 1$ for $I_{a0} = I_{br}$. However, Fig. 3b shows that for $I_{a0} = I_{br}$ and long plasma coupler the output efficiency, η, is slightly reduced, whereas for $I_{a0} = I_{br}/3$ it is largely reduced due to the inverse bremsstrahlung.

Interestingly, Fig. 3c shows that the first spike efficiency is the highest for $I_{a0} = I_{br}/2$ over a large range of plasma coupler lengths, due to a compromise between large Raman growth rate and small dispersion and in-

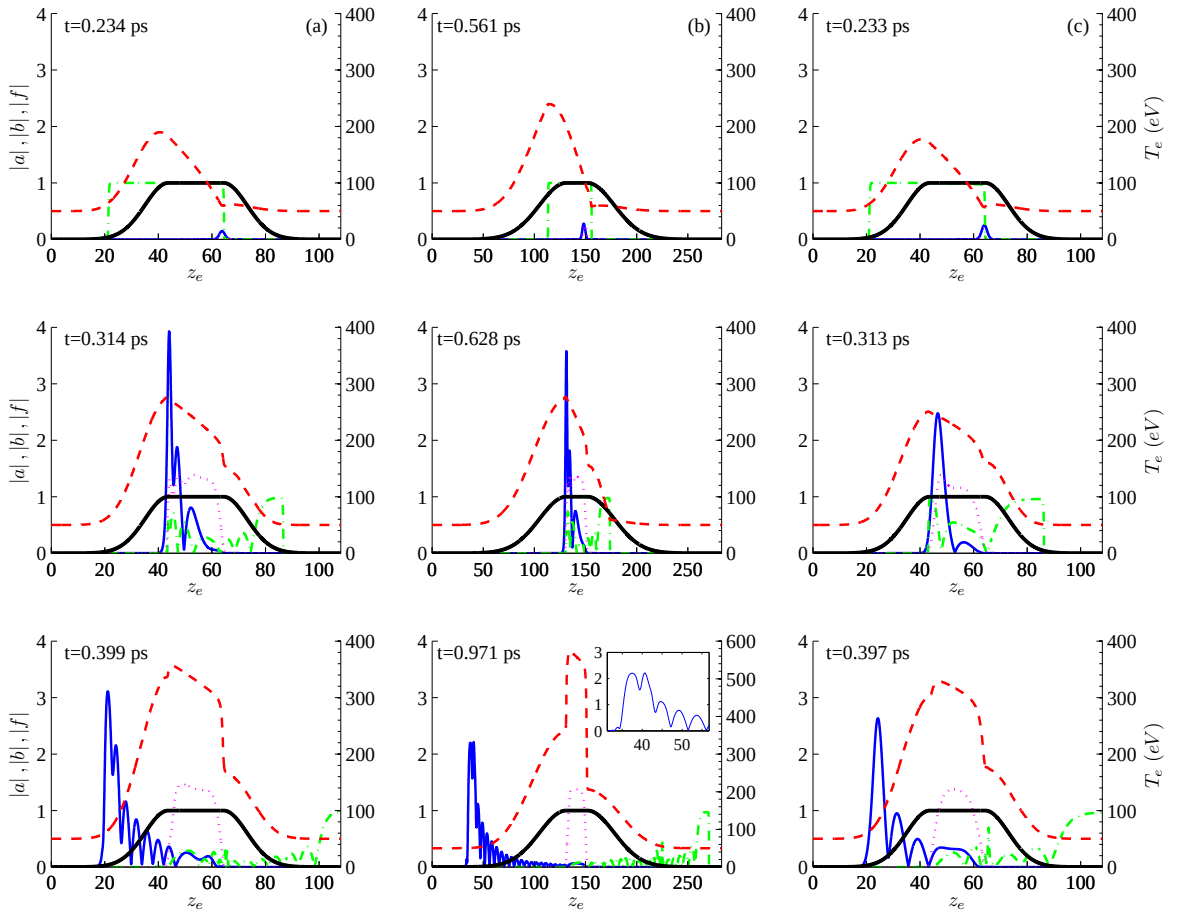

FIG. 1. (Color online) The evolution of the pump, seed, and Langmuir pulses and the electron temperature for $\Delta_n/z_h = 1$ (Figs. 1a and 1c) and $\Delta_n/z_h = 3$ (Fig. 1b). In Figs. 1a and 1c the initial pump intensity is $I_{a0} = I_{br} = 84.55$ PW/cm^2 and in Fig. 1b the initial pump intensity is 28.18 PW/cm^2, which is $I_{a0} = I_{br}/3$. The solid curve is the seed amplitude, the dash-dot curve is the pump amplitude, the dotted curve is the Langmuir amplitude, and the dashed curve is the electron temperature profile. The thick curve is the plasma density profile. Here, z_e is the distance measured in electron plasma wavelength, λ_e. The inset in the bottom of (Fig.1b) is the seed amplitude in the region of its maximum.

verse bremsstrahlung effects. As seen in Figs. 3d, 3e, and 3f, the output intensity, the total output fluence, and the leading spike fluence of the seed are significantly less sensitive to the coupler length for $I_{a0} = I_{br}/2$ than for $I_{a0} = I_{br}$. But for $I_{a0} = I_{br}/2$ the leading spike intensity is about 300 PW/cm^2 and the fluence is 2 kJ/cm^2, compared to intensity of 1000 PW/cm^2 and fluence of 4 kJ/cm^2 for $I_{a0} = I_{br}$ and homogeneous plasma.

IV. DISPERSION AND INVERSE BREMSSTRAHLUNG COMPENSATION BY PUMP AND SEED CHIRPING

To compensate for the dispersion and the inverse bremsstrahlung effects, we suggest to chirp both the pump and seed pulses. In order that the dispersion effect in the plasma couplers be reduced significantly, the pump pulse is also chirped so that the Raman resonance condition is satisfied through the whole plasma layer.

In an inhomogeneous plasma the Raman resonance condition according to Eq. (1) is

$$\omega_a - \omega_b - \omega_e = V_3 a_0(\Delta\omega + \sigma_a + \sigma_b + \sigma_f), \qquad (8)$$

where $\Delta\omega$ is the pump frequency chirp parameter that is required to satisfy Eq. (8). Since in homogeneous plasma the Raman resonance condition is $\omega_a - \omega_b - \omega_e = 0$, the resonance condition in Eq. (8) can be simplified to the form

$$\Delta\omega = \sigma_f + \sigma_b - \sigma_a. \qquad (9)$$

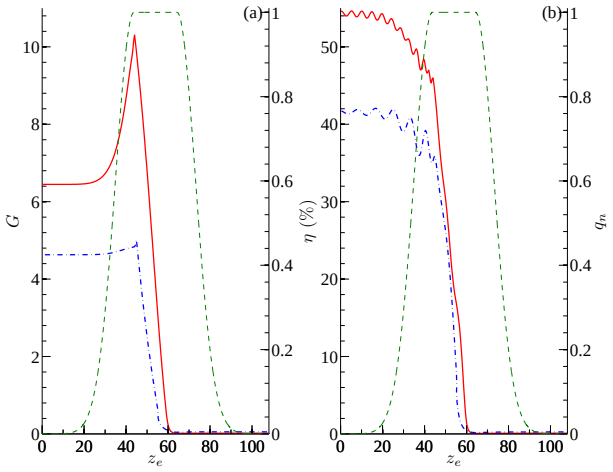

FIG. 2. (Color online) (a) The local gain of the seed pulse for $I_{a0} = I_{br} = 84.55$ PW/cm^2 (solid curve) and $I_{a0} = I_{br}/3 = 28.18$ PW/cm^2(dash-dot curve). (b) The local efficiency of the seed pulse for $I_{a0} = I_{br} = 84.55$ PW/cm^2 (solid curve) and $I_{a0} = I_{br}/3 = 28.18$ PW/cm^2 (dash-dot curve). In both cases $\Delta_n/z_h = 1$. The dashed curve is the plasma density profile.

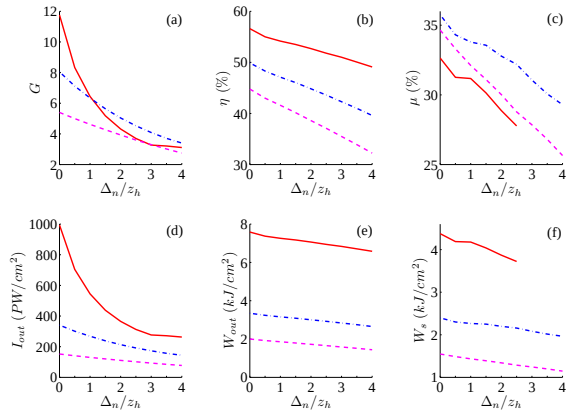

FIG. 3. (Color online) Fig. 3 shows the output gain (a), efficiency (b), and leading spike efficiency (c). The output intensity (d), fluence (e), and leading spike fluence (f) are also shown. The solid curve corresponds to $I_{a0} = I_{br} = 84.55$ PW/cm^2, the dash-dot curve corresponds to $I_{a0} = I_{br}/2 = 42.3$ PW/cm^2, and the dashed curve corresponds to $I_{a0} = I_{br}/3 = 28.18$ PW/cm^2.

We can equivalently chirp the Langmuir pulse, f, with $-\Delta\omega$ chirp parameter. Hence, the equation for the Langmuir pulse becomes

$$f_t = -q_n^{1/4} ab^* + i\sigma_f f - \nu_f f - i\Delta\omega f. \qquad (10)$$

Theoretically, the BRA resonance condition can be satisfied through the whole plasma when chirping the pump pulse according to Eq. 9. However, the input pump intensity at the wave-breaking threshold is small in the inhomogeneous sections where the plasma is tenuous. Hence, to achieve high Raman amplification in most part of the plasma slab, we choose initial pump intensity of $I_{a0} = 24$ PW/cm^2 which is at the wave-breaking threshold for electron density of $5 \cdot 10^{20}$ cm^{-3} ($q_n = 0.5$). In addition, the Gaussian seed pulse is initially chirped so that, in the absence of the pump pulse and the nonlinear relativistic effect, the seed pulse would self-contract for homogeneous density n_h and reach its shortest duration after passing a distance of $1.5z_L = 1.5(z_h + \Delta_n)$, where z_L corresponds to the section of $q_n \geq 0.5$ in the inhomogeneous plasma. The minimum seed duration at this point is $4\pi/\omega_e$ which is the same duration of the non chirped case at the entrance to the plasma. The timing of the pump and the seed pulses were chosen such that the BRA occurs in the section of $q_n \geq 0.5$.

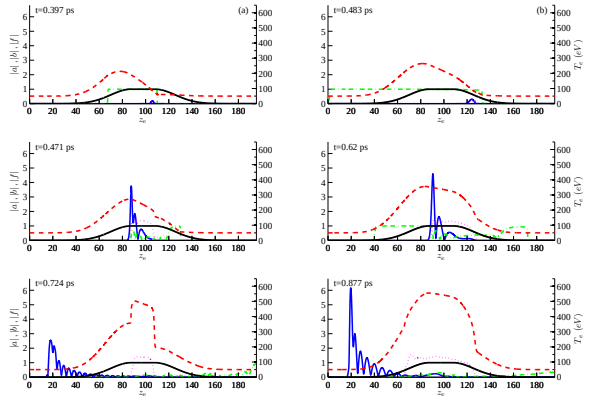

FIG. 4. (Color online) The evolution of the pump, seed, and Langmuir pulses and the electron temperature for (a) chirped pump and seed pulses and for (b) non chirped pump and seed pulses. Solid curve is the seed amplitude, dash-dot curve is the pump amplitude, dotted curve is the Langmuir amplitude, and dashed curve is the electron temperature profile. In both cases $\Delta_n/z_h = 2$. The solid thick curve is the plasma density profile.

Figure 4 compares the evolution of the non chirped pump, non chirped seed, and Langmuir pulse (Fig. 4a) with the chirped pump, chirped seed, and Langmuir pulse (Fig. 4b) for the case of $\Delta_n/z_h = 2$. According to Fig. 4a the output intensity of the amplified non-chirped seed pulse is 365.26 PW/cm^2 with $3 \cdot 2\pi/\omega_e = 10.56$ fsec duration and the leading spike fluence is 3.87 kJ/cm^2. However, the output intensity of the amplified chirped seed pulse (Fig. 4b) is 608 PW/cm^2 with $1.88 \cdot 2\pi/\omega_e = 6.62$ fsec duration. The leading spike fluence is 4 kJ/cm^2. Also, the secondary spikes of the amplified chirped seed pulse are much smaller than in the non chirped seed pulse. These secondary spikes are also not close to the leading spike. Thus, the output pulse is significantly reshaped.

To see in more detail the amplification and efficiency

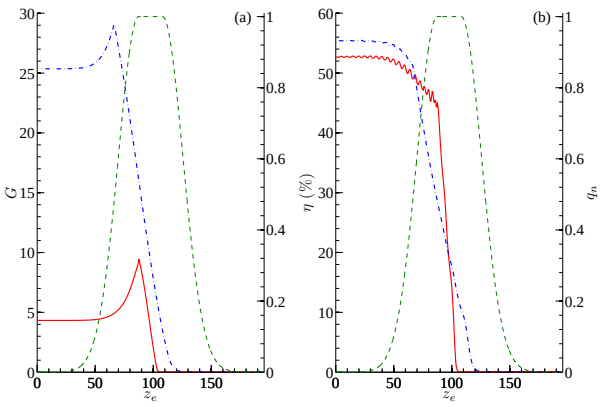

FIG. 5. (Color online) (a) The local gain of the seed pulse for non chirped pump and seed pulses (solid curve) and for chirped pump and seed pulses (dash-dot curve). (b) The local efficiency of the seed pulse for non chirped pump and seed pulses (solid curve) and for chirped pump and seed pulses (dash-dot curve). In both cases $\Delta_n/z_h = 2$.

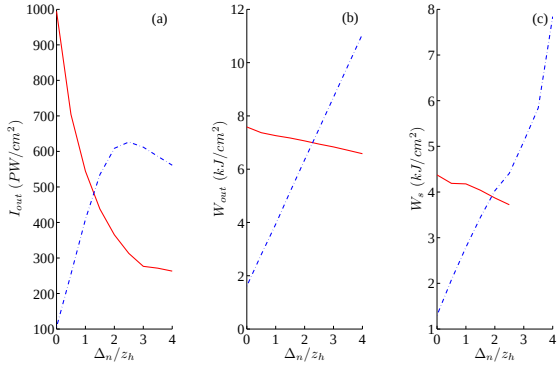

FIG. 6. (Color online) Fig. 6 shows the output intensity (a), fluence (b), and leading spike fluence (c). The solid curve corresponds to non chirped pump and seed pulses and the dash-dot curve corresponds to chirped pump and seed pulses.

of the chirped seed pulse in this example, we show in Fig. 5(a) the local gain and in 5(b) the local fluence efficiency. Also, we compared the non chirped seed (solid curve and it is the same as in Fig. 2) with the chirped seed and pump (dash-dot curve). As can be seen from Figs. 5a and 5b, the Raman amplification occurs over longer distance for the chirped seed and pump ($q_n \leq 0.5$) than the non-chirped seed and pump ($q_n = 1$). In this example, the output intensity of the chirped seed and pump is 608 PW/cm^2, which is higher by 65% than the intensity of the non-chirped seed pulse which is 365.26 PW/cm^2. The total efficiency is similar, about 55%, with a bit higher efficiency for the chirped seed pulse. The output fluence of the first spike of the seed is about 4 kJ/cm^2.

Since for the chirped seed and pump the amplification stopped at the point where the plasma density is half that in the homogeneous region, the seed pulse profile after the amplification was significantly less affected both by the dispersion and the inverse bremsstrahlung. However, the smaller Raman growth rate in the case of the chirped seed case requires a longer plasma coupler to achieve output intensity and efficiency larger than in the case of the non-chirped seed and pump.

Figs. 6a and 6b show the dependence of the output intensity and fluence on the plasma coupler length. As seen in Figs. 6a and 6b, the output intensity and fluence of the chirped seed (dash-dot curve) is larger than the non-chirped seed for plasma coupler length at least twice the length of the homogeneous section ($\Delta_n/z_h \geq 2$).

V. CONCLUSIONS

We considered Raman compression in a plasma slab which is comprised of a homogeneous middle section and inhomogeneous end sections, such that the electron density in each end section tapers to zero. In our specific example the pump wavelength is 0.351 μm and the electron density in the homogeneous section is 10^{21} cm^{-3}, corresponding to $\omega_e/\omega_a = 0.33$. Though it is a specific example, it indicative of the general case of undercritical dense plasma, where both seed dispersion and inverse bremsstrahlung can be limiting effects.

We showed, for initial pump intensity at the wavebreaking threshold, a significant reduction in the output seed amplification for plasma coupler length longer than the homogeneous section. The amplification is strongly reduced at the exit of the homogeneous section, where the seed pulse duration is the shortest and hence the seed dispersion is the strongest. Nevertheless, the output fluence is almost not affected since the dispersion is non-dissipative. For lower initial pump intensity, hence lower Raman growth rate, the seed amplitude is smaller and its duration longer. Hence, the seed dispersion is smaller in the exit plasma coupler which results in a smaller reduction of the seed amplitude and fluence. However, the output amplification and fluence are smaller than in the case of initial pump intensity at the wavebreaking threshold.

Interestingly, we showed that the first spike efficiency is highest for $I_{a0} = I_{br}/2$ over a large range of plasma coupler lengths. The maximum occurs because of a compromise between large Raman growth rate and small dispersion and inverse bremsstrahlung effects. However, the leading spike intensity and fluence are significantly smaller than the initial pump intensity at the wavebreaking threshold in homogeneous plasma.

To compensate for the dispersion and inverse bremsstrahlung effects, we propose to chirp both the pump and the seed pulses such that the BRA will be in resonance over a longer plasma length which includes both the homogeneous section and part of the inhomogeneous sections. While in the case of non chirped pump and seed, the Raman compression stops at the edge of

the homogeneous section, in this approach the Raman compression continues in the end region and stops at the point where the plasma density is half that of the homogeneous section. Thus, the seed dispersion is significantly smaller than in the case of the non chirped pump and seed. We showed that for plasma coupler longer than the homogeneous section the output chirped seed pulse can reach higher intensity and fluence than in the case of the non chirped pump and seed.

The case of long end-regions is important for the next generation of power which will require larger spot-sizes or cross sections for the Raman compression. These cross sections will be larger compared to the desired width of the plasma slab, which remains fixed. For large cross sections and small widths, the plasma density will likely taper to zero over a distance large compared to its optimum width, thus creating the conditions wherein the measures proposed here may be useful.

ACKNOWLEDGMENTS

This work was supported by the NNSA under the SSAA Program through DOE Research Grant No. DE-AC0209-CH11466, by the RFBR Grant No. 11-02-01070, and by the RFBR Grant No. 12-02-00650.

[1] V. M. Malkin, G. Shvets, and N. J. Fisch, Phys. Rev. Lett. **82**, 4448 (1999).
[2] D. Strickland and G. Mourou, Opt. Commun. **56**, 219 (1985).
[3] M. S. Hur, R. R. Lindberg, A. E. Charman, J. S. Wurtele, and H. Suk1, Phys. Rev. Lett. **95**, 115003 (2005).
[4] M. S. Hur, D. N. Gupta, and H. Suk, J. Phys. D **40**, 5155 (2007).
[5] M. S. Hur and J. S. Wurtele, Comp. Phys. Comm. **180**, 651 (2009).
[6] T.-L. Wang, D. S. Clark, D. J. Strozzi, S. C. Wilks, S. F. Martins, and R. K. Kirkwood, Phys. Plasmas **17**, 023109 (2010).
[7] H. Gareth, S. Ashutosh, and K. Ioannis, Phys. Lett. A **374**, 4336 (2010).
[8] S. Son, S. Ku, and S. J. Moon, Phys. Plasmas **17**, 114506 (2010).
[9] D. Benisti, O. Morice, L. Gremillet, E. Siminos, and D. J. Strozzi, Phys. Plasmas **17**, 102311 (2010).
[10] J. P. Farmer, B. Ersfeld, and D. A. Jaroszynski, Phys. Plasmas **17**, 113301 (2010).
[11] V. V. Kozlov, S. V. Manakov, and S. Wabnitz, Opt. Lett. **36**, 1632 (2011).
[12] G. Zhe-Yi, Y. Yan, C. De-Peng, Z. Hong-Bin, M. Yan-Yun, and S. Fu-Qiu, Chin. Phys. Lett. **29**, 015201 (2012).
[13] N. A. Yampolsky and N. J. Fisch, Phys. Plasmas **18**, 056711 (2011).
[14] G. A. Mourou, N. J. Fisch, V. M. Malkin, Z. Toroker, E. A. Khazanov, A. M. Sergeev, T. Tajima, and B. L. Garrec, Opt. Commun. **285**, 720 (2012).
[15] D. S. Clark and N. J. Fisch, Phys. Plasmas **8**, 3363 (2003).
[16] N. J. Fisch and V. M. Malkin, Phys. Plasmas **10**, 2056 (2003).
[17] V. M. Malkin, G. Shvets, and N. J. Fisch, Phys. Plasmas **12**, 044507 (2005).
[18] V. M. Malkin, G. Shvets, and N. J. Fisch, Phys. Rev. E **75**, 026404 (2007).
[19] A. A. Balakin, N. J. Fisch, G. M. Fraiman, V. M. Malkin, and Z. Toroker, Phys. Plasmas **18**, 102311 (2011).
[20] A. A. S. V. M. Malkin and N. J. Fisch, Phys. Plasmas **10**, 2540 (2003).
[21] V. M. Malkin and N. J. Fisch, Phys. Plasmas **17**, 073109 (2010).
[22] R. M. G. M. Trines, F. Fiuza, R. Bingham, R. A. Fonseca, L. O. Silva, R. A. Cairns, and P. A. Norreys, Nature Phys. **7**, 87 (2011).
[23] R. M. G. M. Trines, F. Fiuza, R. Bingham, R. A. Fonseca, L. O. Silva, R. A. Cairns, and P. A. Norreys, Phys. Rev. Lett. **107**, 105002 (2011).
[24] V. M. Malkin, Z. Toroker, and N. J. Fisch, Phys. Plasmas **19**, 023109 (2012).
[25] V. M. Malkin and N. J. Fisch, Phys. Rev. Lett. **99**, 205001 (2007).
[26] V. M. Malkin, G. Shvets, and N. J. Fisch, Phys. Rev. Lett. **7**, 1208 (2000).
[27] M. N. Rosenbluth, Phys. Rev. Lett. **29**, 565 (1972).
[28] A. A. Balakin, D. V. Kartashov, A. M. Kiselev, S. A. Skobelev, A. N. Stepanov, and G. M. Fraiman, JETP Lett. **80**, 12 (2004).
[29] X. Yang, G. Vieux, E. Brunetti, J. P. Farmer, B. Ersfeld, S. M. Wiggins, R. C. Issac, G. H. Welsh, and D. A. Jaroszynski, Proc. SPIE **8075**, 80750G (2011).
[30] G. Vieux, A. Lyachev, X. Yang, B. Ersfeld, J. P. Farmer, E. Brunetti, R. C. Issac, G. Raj, G. H. Welsh, S. M. Wiggins, and D. A. Jaroszynski, New J. Phys. **13**, 063042 (2011).
[31] R. K. Kirkwood, E. Dewald, C. Niemann, N. Meezan, S. C. Wilks, D. W. Price, O. L. Landen, J. Wurtele, A. E. Charman, R. L. N. J. Fisch, V. M. Malkin, and E. J. Valeo, Phys. Plasmas **14**, 113109 (2007).
[32] J. Ren, S. Li, A. Morozov, S. Suckewer, N. A. Yampolsky, V. M. Malkin, and N. J. Fisch, Phys. Plasmas **15**, 056702 (2008).
[33] Y. Ping, I. Geltner, N. J. Fisch, G. Shvets, and S. Suckewer, Phys. Rev. E **62**, R4532 (2000).
[34] Y. Ping, I. Geltner, A. Morozov, N. J. Fisch, and S. Suckewer, Phys. Rev. E **66**, 046401 (2002).
[35] Y. Ping, W. Cheng, S. Suckewer, D. S. Clark, and N. J. Fisch, Phys. Rev. Lett. **92**, 175007 (2004).
[36] W. Cheng, Y. Avitzour, Y. Ping, S. Suckewer, N. J. Fisch, M. S. Hur, and J. S. Wurtele, Phys. Rev. Lett. **94**, 045003 (2005).
[37] C. H. Pai, M. W. Lin, L. C. Ha, S. T. Huang, Y. C. Tsou, H. H. Chu, J. Y. Lin, J. Wang, and S. Y. Chen, Phys. Rev. Lett. **101**, 065005 (2008).
[38] K. Mima, M. M. Skoric, S. Miyamoto, A. Maluckov, and M. S. Jovanovic, AIP Conf. Proc. **406**, 381 (1997).
[39] W. L. Kruer, *The Physics of Laser Plasma Interactions* (Addison-Wesley, Reading, MA, 1988).
[40] A. G. Litvak, Zh. Eksp. Teor. Fiz. [Sov. Phys. JETP] **57 [30]**, 629 [344] (1969 [1970]).
[41] C. Max, J. Arons, and A. B. Langdon, Phys. Rev. Lett **33**, 209 (1974).
[42] G.-Z. Sun, E. Ott, Y. C. Lee, and P. Guzdar, Phys. Fluids **30**, 526 (1987).
[43] A. Balakin, G. Fraiman, and V. Mironov, Phys. Plasmas **8**, 2502 (2001).
[44] A. Brantov, W. Rozmus, and R. Sydora, Phys. Plasmas **10**, 3385 (2003).
[45] G. L. Lamb-Jr., Phys. Lett. A **29**, 507 (1969).
[46] G. L. Lamb-Jr., Rev. Mod. Phys. **43**, 99124 (1971).
[47] G. L. Lamb-Jr., *Elements of Soliton Theory* (Wiley, New York, 1980).
[48] V. E. Zakharov, JETP Lett. **32**, 589 (1980).
[49] S. V. Manakov, JETP Lett. **35**, 237 (1982).
[50] V. A. Gorbunov, V. B. Ivanov, S. B. Papernyi, and V. R. Startsev, Izv. Akad. Nauk SSSR, Ser. Fiz. [Bull. Acad. Sci. USSR, Phys. Ser. (Engl. Transl.)] **48**, 1580 [120] (1984).
[51] J. Coste and C. Montes, Phys. Rev. A **34**, 3940 (1986).

The Princeton Plasma Physics Laboratory is operated
by Princeton University under contract
with the U.S. Department of Energy.

Information Services
Princeton Plasma Physics Laboratory
P.O. Box 451
Princeton, NJ 08543

Phone: 609-243-2245
Fax: 609-243-2751
e-mail: pppl_info@pppl.gov
Internet Address: http://www.pppl.gov